SCIENTIFIC REPORTS

OPEN

The development of fluorescence turn-on probe for Al(III) sensing and live cell nucleus-nucleoli staining

Anoop Kumar Saini[1], Vinay Sharma[2], Pradeep Mathur[1] & Mobin M. Shaikh[1,2,3]

The morphology of nucleus and nucleolus is powerful indicator of physiological and pathological conditions. The specific staining of nucleolus recently gained much attention due to the limited and expensive availability of the only existing stain "SYTO RNA-Select". Here, a new multifunctional salen type ligand (L_1) and its Al^{3+} complex (**1**) are designed and synthesized. L_1 acts as a chemosensor for Al^{3+} whereas **1** demonstrates specific staining of nucleus as well as nucleoli. The binding of **1** with nucleic acid is probed by DNase and RNase digestion in stained cells. **1** shows an excellent photostability, which is a limitation for existing nucleus stains during long term observations. **1** is assumed to be a potential candidate as an alternative to expensive commercial dyes for nucleus and nucleoli staining.

Recent advancement and development in fluorescence imaging techniques has witnessed tremendous upsurge in the field of metal ion sensing and live cell imaging[1–5]. The sensitive bio-imaging of Al^{3+} in various cell lines can be helpful for understanding the fundamental mechanism of aluminium-induced human diseases. The widespread prevalence of Aluminium and its serious health threats such as Parkinson's disease, Kidney damage and Alzheimer's disease makes it imperative to develop Al(III) sensors[6–10]. Tolerable limit of Al^{3+} in human is estimated to be around 7 mg Kg^{-1} per week[11]. The conventional methods for Al^{3+} detection like inductively coupled plasma-atomic emission spectrometry (ICP-AES), atomic absorption spectrometry (AAS) and inductively coupled plasma-mass spectrometry(ICP-MS) are relatively expensive and suffers from lack of selectivity, sensitivity and interferences generated from the matrix[12]. However, spectrofluorimetry technique is superior in terms of quick analysis, high selectivity, sensitivity and ease of operation[13]. On the other hand, the critical role of cell nucleus in various cellular events like metabolism, reproduction and heredity highlights the importance of nucleus staining agents for determining the morphology and functionality of nucleus[14]. The existing nuclear staining agents like DAPI and Hoechst suffers from photo-bleaching and self-quenching which limits their applicability for long term observations[15,16]. The nucleolus is an important sub-nuclear structure and its dynamic morphology is indicative of pathological and physiological situations[17]. The inability of DAPI and Hoechst to stain nucleolus and limitations of extremely expensive existing nucleolus stains emphasize the requirement of a total nucleus staining dye. Hence, the development of new generation of low cytotoxic and high photostable nucleus staining agent[16] as well as selective and sensitive sensor for intracellular detection of trace amount of Al^{3+} accorded significant attention[18–20].

There are few reports on specific staining of nucleus by employing nano-materials[21] and Ir(III)[14]/ Ru(II)[15] complexes to different cell lines. Specific staining of nucleolus is also achieved using carbon based nano-materials[22], nanoclusters[23], coumarin and pyronin based moieties[24,25], Eu(III)[26]/Ir(III)[27] complexes and semiconducting quantum dots[28]. Two water soluble molecules containing N-methyl benzothiazolium moiety are recently reported which individually stains nucleus and nucleolus[29]. There exists only few commercial dye(s) which specifically stains nucleoli but has some limitations like specific storage requirements, toxicity, rare availability and expensiveness[14]. However, to the best of our knowledge, so far no report is available on specific nucleus as well as nucleoli staining using **1**.

Herein, we report synthesis of multifunctional ligand L_1 and its Al^{3+} complex (**1**) for specific nucleus and nucleoli staining along with sensitive intracellular Al^{3+} detection.

[1]Discipline of Chemistry, Indian Institute of Technology Indore, Simrol, Indore 453552, India. [2]Centre for Biosciences and Bio-Medical Engineering, Indian Institute of Technology Indore, Simrol, Indore 453552, India. [3]Metallurgical Engineering and Material Science, Indian Institute of Technology Indore, Simrol Indore 453552, India. Correspondence and requests for materials should be addressed to M.M.S. (email: xray@iiti.ac.in) or P.M. (email: director@iiti.ac.in)
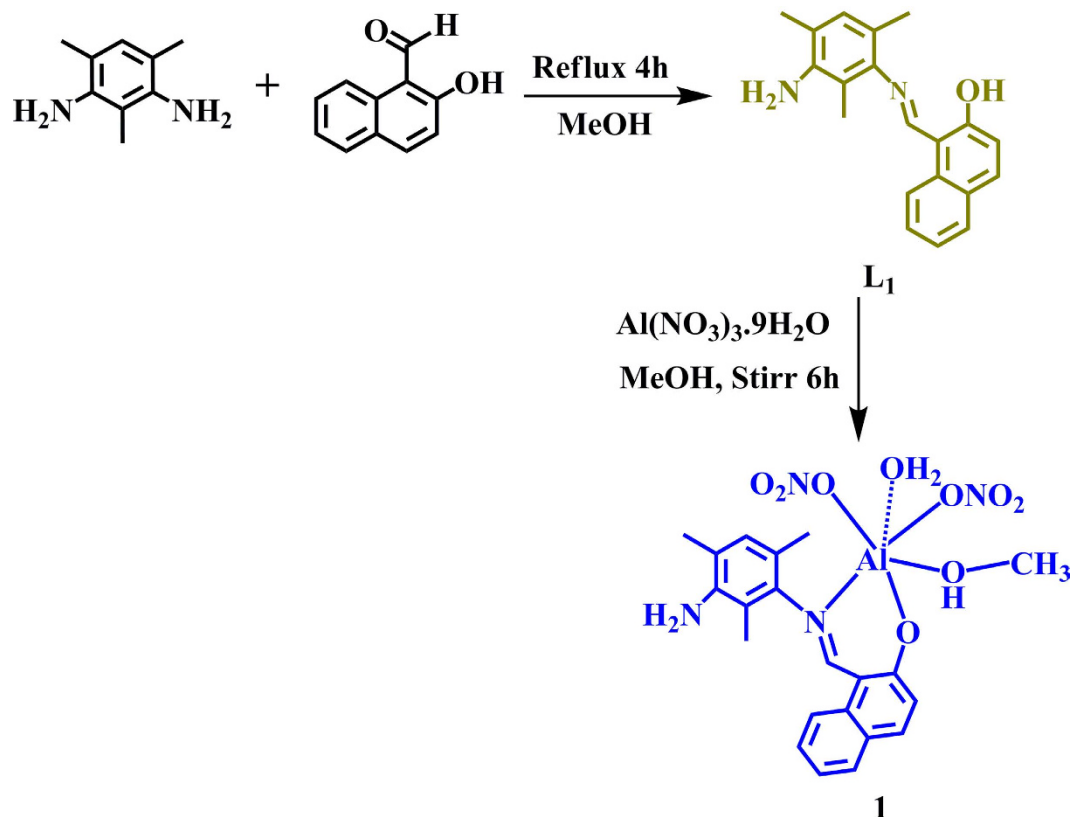
**Figure 1. Synthesis of ligand L$_1$ and 1.**

Results

We recently reported synthesis of a highly selective, sensitive and reversible symmetric chemosensor H$_2$L for Zn^{2+} ion (Supplementary Fig. S1)[30]. Encouraged by the results, we have slightly altered the ratio of 2,4,6-trimethylbenzene-1,3-diamine and 2-Hydroxy-1-napyhaldehyde to 1:1 (Fig. 1) instead of 1:2 ratio, which results in another chemosensor (**L$_1$**) for selective and sensitive detection of Al^{3+}.

L$_1$ is characterized by elemental analysis, HRMS, NMR and further authenticated by single crystal X-ray studies. Furthermore, the reaction of **L$_1$** with Al(NO$_3$)3.9H$_2$O in presence of methanol at room temperature yields complex **1** (Fig. 1). **L$_1$** crystallize in monoclinic *P2$_1$/n* space group (Supplementary Fig. S2 and Supplementary Table S1). The packing of **L$_1$** reveals intermolecular H-bonding interaction and C-H···π interaction[31] forming hydrogen bonded 2D-network (Supplementary Fig. S3 and Supplementary Table S2).

**Photophysical properties.** The absorption spectra of **L$_1$** shows absorption peaks at 309 nm and 360 nm corresponding to n-π* and at 419 nm corresponding to π-π* transition. Upon subsequent addition of increasing concentration of Al^{3+} ions, the absorbance intensity gradually enhanced at 419 nm and decreased at 309 and 360 nm having one isosbestic point at 391 nm (Fig. 2(a)) with change in color from *yellow* to *blue* under UV light. However, addition of varying concentrations of other metal ions viz.; Ag$^+$, Na$^+$, K$^+$, Li$^+$, Mn^{2+}, Cd^{2+}, Hg^{2+}, Mg^{2+}, Ca^{2+}, Cr^{3+}, Ni^{2+}, Co^{2+}, Cu^{2+}, Zn^{2+}, Pb^{2+}, Fe^{2+} and As^{3+} to the **L$_1$** solution results in no significant change in the absorbance and color (Fig. 2(b), Supplementary Fig. S4).

The emission studies of **L$_1$** at excitation wavelength 309 nm, shows weak fluorescence at 341 nm which is attributed to the isomerization of the imine bond (−HC=N) and excited state intramolecular proton transfer (ESIPT) from the −OH group to the imine nitrogen[30]. The titration of **L$_1$** with Al^{3+} shows gradual fluorescence enhancement with a bathochromic shift (red shift) of 2 nm having maximum fluorescence intensity at 343 nm. Also, emergence of two more emission peaks at 351 and 448 nm is observed (Fig. 2(c)).

The probable reason for the fluorescence switch on towards Al^{3+} may be due to (i) the photoinduced electron transfer (PET) suppressed by Al^{3+} coordination and (ii) new band in absorption spectrum[32]. PET shows changes in emission intensities with some or no spectral shifts. In our case, the spectral shift is of 2 nm in emission maxima during the fluorescence titration. The shorter fluorescence lifetime and lower quantum yield also support the operation of PET process[33,34]. The schematic representation of working mechanism is shown in Supplementary Fig. S5. Thus, the results obtained from absorption and emission studies validate that the sensing behavior of **L$_1$** is specific to Al^{3+} ions. The binding affinity of **L$_1$** with Al^{3+} is found to be 1.18×10^5 M^{-1} and 1.21×10^5 M^{-1} by absorption and emission methods, respectively by using Benesi-Hildebrand equation[35,36] (Supplementary Fig. S6). The limit of detection (LOD) is found to be 86 nM. In general, chemosensor suffer with long response time[37–39]. In our case, the binding of Al(III) towards **L$_1$** is found to be very fast. After adding the aqueous solution of Al(III) to **L$_1$**, the fluorescence intensity at 343 nm reached maximum within 120 s (Supplementary Fig. S7).
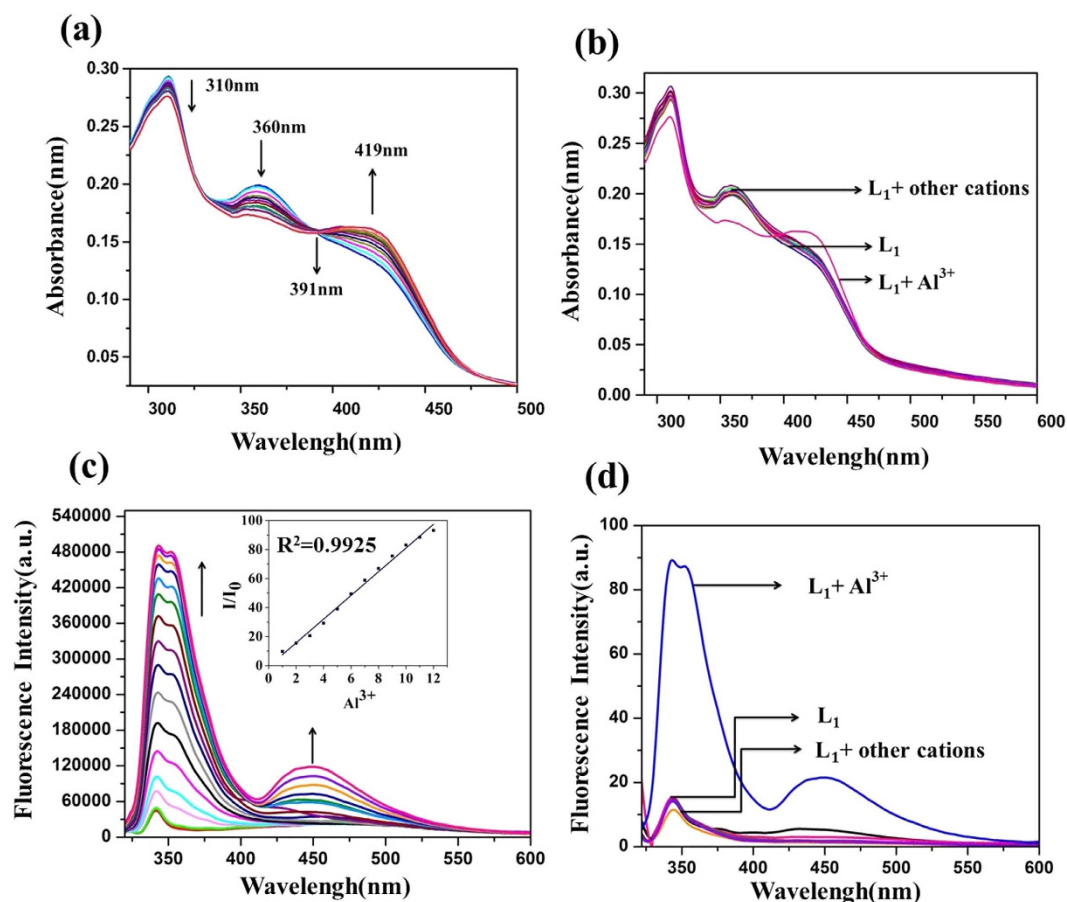
Figure 2. (a) UV-vis absorption titration spectra of L_1 v/s Al^{3+}. (b) Competitive absorption spectra of L_1 in presence of different metal ions, (c) Fluorescence emission spectra obtained by the titration of L_1 inset: shows the relative fluorescence intensity (I/I_0) as a function of $[Al^{3+}]/[L_1]$ mole ratio and (d) Effect of fluorescence intensity at 343 nm with addition of Al^{3+} along with other metal ions. (Conditions: (L_1, $c = 1.0 \times 10^{-5}$ M) in aq. ACN (ACN/H_2O = 7:3 v/v, 10 μM HEPES buffer, pH = 7.4) with Al^{3+} ion($c = 1.0 \times 10^{-4}$ M).
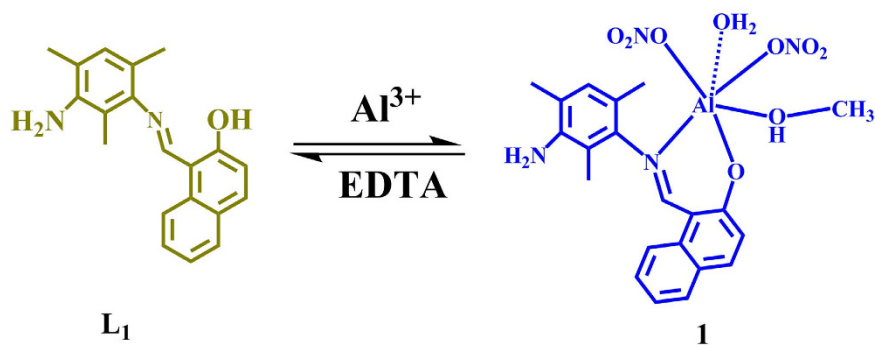
Figure 3. Schematic representation showing reversible nature of chemosensor L_1.

Selectivity, reversibility and mode of binding. Further, the selectivity test is performed using various metal ions with L_1 which shows that only Al^{3+} ion exhibits fluorescence turn on (Fig. 2(d) and Supplementary Fig. S8(a)). A competitive selectivity test was also performed for various metal ions in presence of Al^{3+} in 1:4 ratio which shows that the presence of other metal ion do not affect the selective Al^{3+} sensing behavior of L_1 (Supplementary Fig. S8(b)). The interference of DNA in the probe's ability to detect Al(III) was examined and it was found that the DNA does not interfere with the sensing property of L_1 (Supplementary Fig. S9). For validating the reversibility, the chemosensor L_1 is studied by employing EDTA as a chelating agent. The increased fluorescence intensity of L_1 with Al^{3+} ion was quenched by addition of EDTA (Fig. 3 and Supplementary Fig. S10).

Further, to understand the mode of complexation of L_1 with Al^{3+} ion, ^{1}H NMR titration is performed in DMSO-D6 and D_2O solvents. On subsequent addition of Al^{3+} to L_1, the napthyl –OH peak (15.34 ppm) decreases
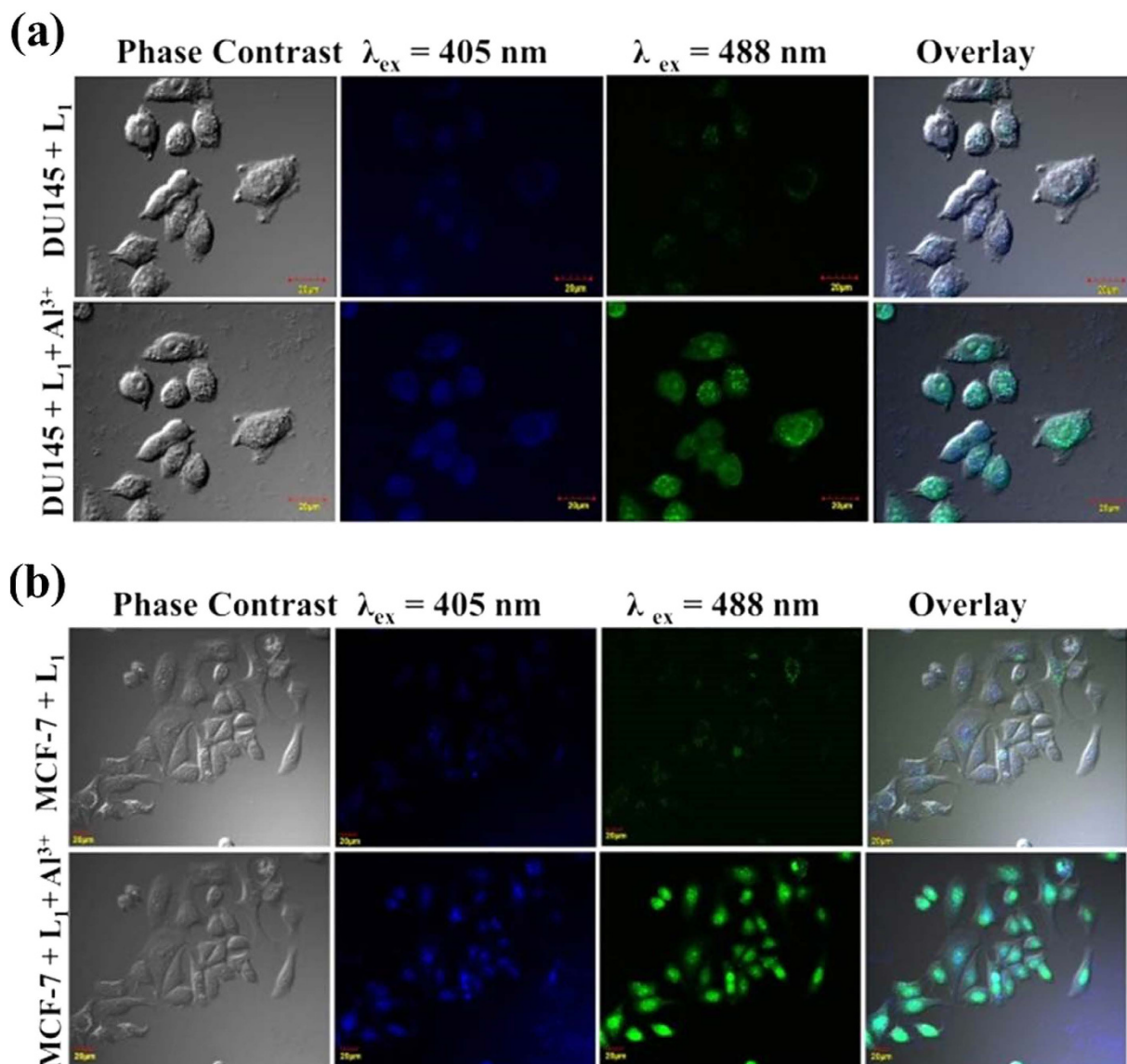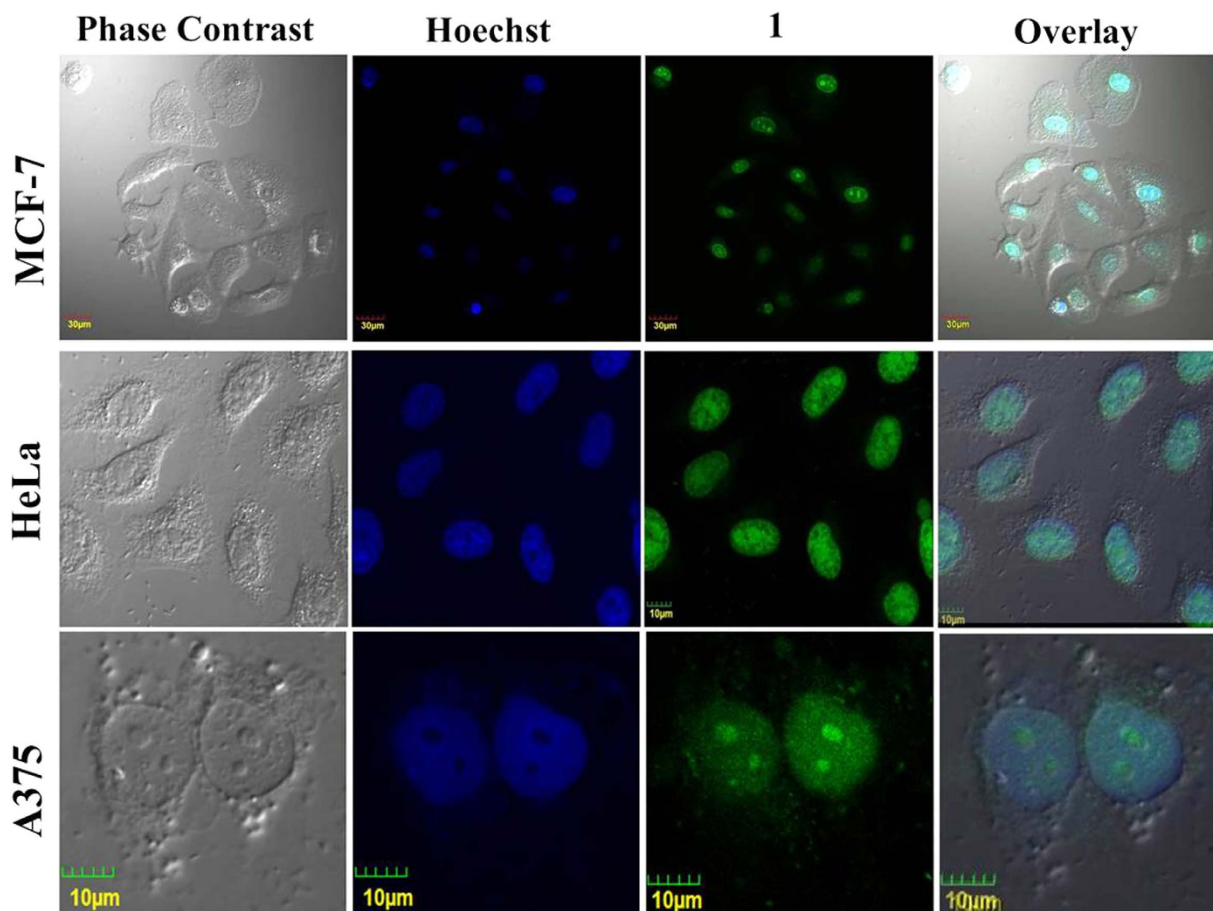
Figure 4. Intracellular Al^{3+} sensing in cancer cell lines (**a**) DU145 (**b**) MCF-7. (Excitation: 405 nm, Emission: 415–470 nm; Excitation: 488 nm, Emission: 500–550 nm).

and finally at 0.8 eq. of Al^{3+}, $-OH$ peak was completely diminished which indicates complex formation of L_1 with Al^{3+} (Supplementary Fig. S11). The stoichiometry of **1** is also confirmed by Job's method which indicates 1:1 complex formation of L_1 with Al^{3+} (Supplementary Fig. S12).

The optical properties of **1** results in high quantum yield ($\Phi = 0.172$) with average life time $<\tau> = 0.99$ ns. (Supplementary Figs S13, S14 and Supplementary Tables S3, S4). The performance comparison of L_1 with other available fluorescent probes for Al^{3+} sensing is shown in Supplementary Table S5.

Cytotoxicity assessment.   To understand the practical ability of L_1 and **1** as a sensor for biological systems, it is obvious to study the cytotoxicity. The cytotoxicity studies are carried out using MTT assay[40]. Human prostate cancer cell line DU145 is incubated with L_1 and **1** (0.01–100 μM) for 24 h and the cell viability is quantified. The results summarized in Supplementary Fig. S15, indicates the cytocompatibility of the probe L_1 and **1**. The cell viability is more than 80% at a high concentration of 100 μM which represent very low cytotoxicity of L_1 and **1**.

Intracellular Al^{3+} sensing.   The excellent sensing response and low cytotoxicity of L_1, prompted us to explore for intracellular Al^{3+} sensing using confocal laser scanning microscopy. In this regard, two cell lines, DU145 and MCF-7 were first treated with 10 μM of L_1 and incubated for 45 minutes at 37 °C. These L_1 treated cells are subjected to confocal microscopy and were excited using lasers wavelength of 405nm and 488nm. As depicted in Fig. 4, the cells treated with L_1 resulted in a very weak intracellular fluorescence with blue and green colored signal at different excitation with uneven distribution in the cells. On addition of 10 μM of Al^{3+} to these cells, a considerable enhancement in blue and green colored fluorescent signal was observed. This confirms the ability
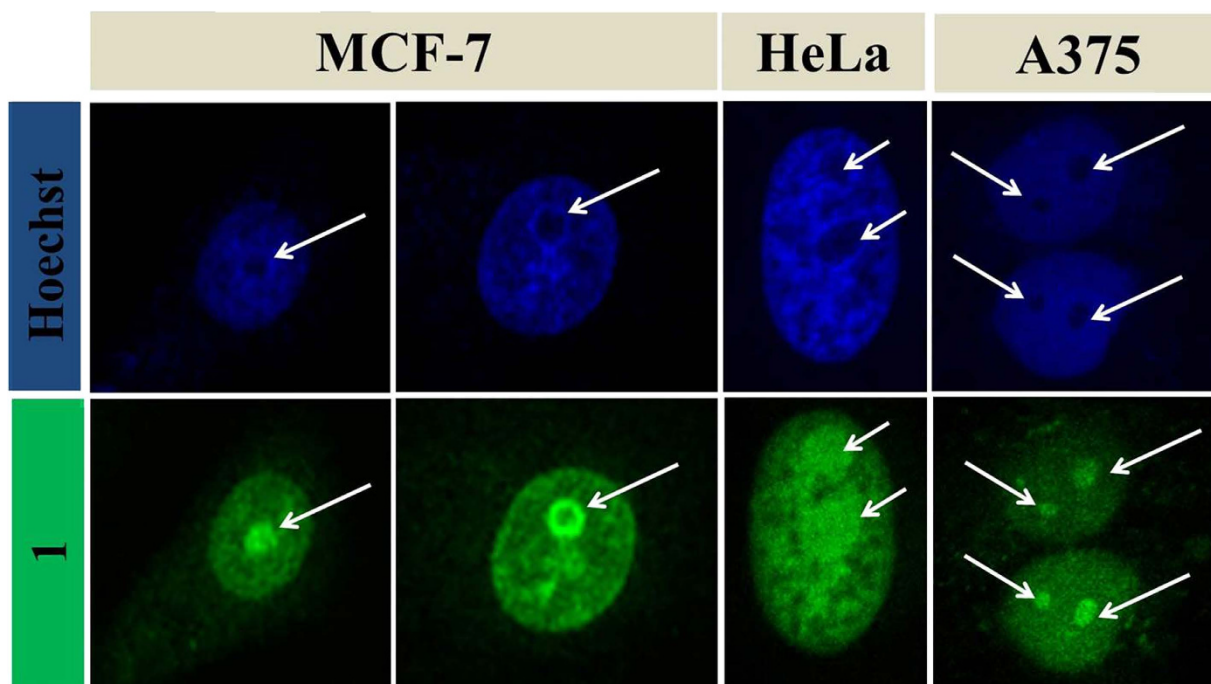
Figure 5. Nucleus specific staining using 1 in breast cancer cell line MCF-7, cervical cancer cell line HeLa and skin melanoma A375. (Excitation: 405 nm, Emission: 415–470 nm; Excitation: 488 nm, Emission: 500–550 nm).

of L_1 to probe intracellular Al^{3+} and a possible intracellular multicolor bioimaging potential of **1**. Moreover, to our surprise, it is observed that the fluorescence signal becomes confined to the nuclei after some time (within 10 minutes), which hinted towards the possible nuclei specificity of **1**, which was further explored. The wavelength tuned emission spectra of **1** was recorded, which shows bathochromic shift with increase in excitation wavelength (Supplementary Fig. S16) resulting into multicolor bioimaging property. The similar wavelength tuned emission behavior of fluorophores is shown in previous reports[5,41–43].

Nucleus and nucleolus specific staining. The interesting intracellular sensing response by L_1 and hint of nucleus targeting by **1**, provoked us to study the bioimaging potential of **1**. The breast cancer cell line MCF-7, cervical cancer cell line HeLa and skin melanoma cell line A375 is used for comparison between the staining ability of a standard nucleus stain and **1**. These cells are first stained with Hoechst 33342 and the emission is recorded at $\lambda_{ex} = 405$ nm Further, 20 μM of **1** is added and after 5 minutes incubation, the intracellular emission is recorded at $\lambda_{ex} = 488$ nm. The blue fluorescence from nucleus specific Hoechst dye is completely overlapped by the nucleus staining green fluorescence of **1** (Fig. 5, Supplementary Fig. S17). The strong overlap validated the potential of **1** as a specific nucleus stain. The Pearson's colocalisation coefficient was obtained to be $R_r = 0.75$ (Supplementary Fig. S18), which is in close agreement with recently reported nucleic acid selective probes[29].

It is worth to mention that the dual staining experiment was performed in serial "staining and imaging" mode. First, the cells were stained with Hoechst and the fluorescence emission was recorded in blue channel in absence of **1** to avoid excitation of **1** in blue channel. Further, **1** was added without disturbing the cell position and the emission was recorded in green channel to avoid any interference with Hoechst fluorescence.

A closer look at the comparative nucleus stain of Hoechst and **1**, exhibits the dominance of **1** in not only staining nucleus but also nucleolus, which remains unstained in case of Hoechst as demonstrated in Fig. 6. To study intracellular photostability of **1**, the MCF-7 cells are stained with **1** and a dual channel emission video is recorded upto 450 scans, where laser of 405 and 488 nm is triggered at every scan (Supplementary Video 1). The video shows no obvious photobleaching, which suggests high photostability and feasibility of **1** as an efficient and suitable candidate for total nucleus stain. The fluorescence stability of **1** is also tested under continuous UV illumination up to two hours and varied temperature in range of (−80 °C to 90 °C), which shows high photostability

Figure 6. Nucleolus staining using 1 in breast cancer cell line MCF-7, cervical cancer cell line HeLa and skin melanoma A375. (Excitation: 405 nm, Emission: 415–470 nm; Excitation: 488 nm, Emission: 500–550 nm).
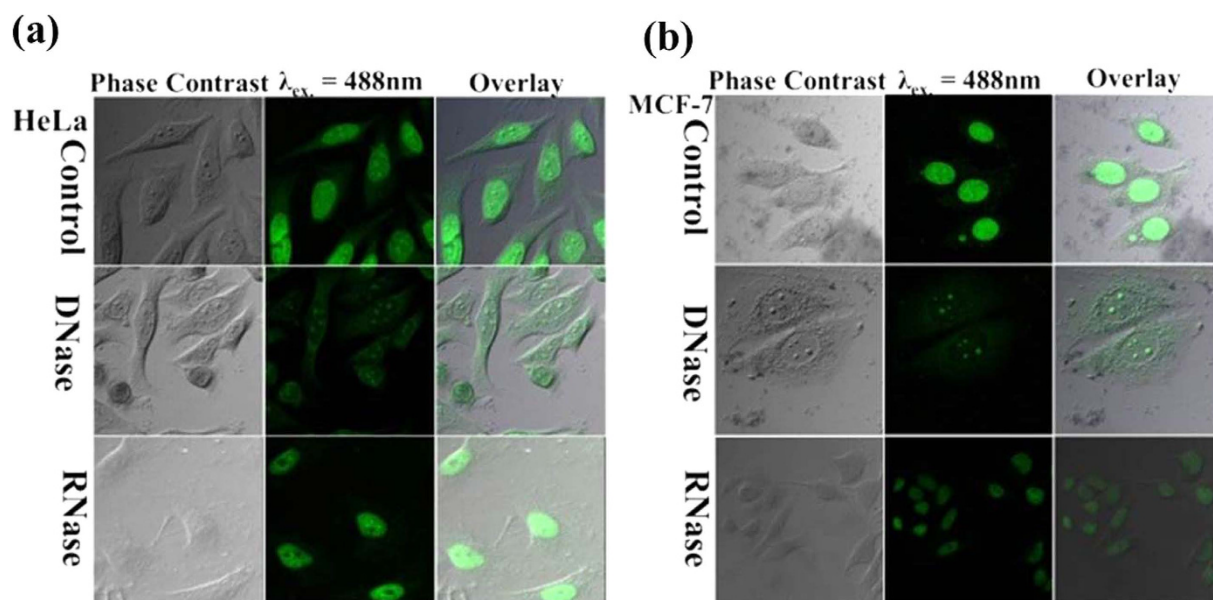
Figure 7. DNase and RNase digestion test in MCF-7, HeLa cell lines. (Excitation: 488 nm, Emission: 500–550 nm).

of **1** (Supplementary Fig. S19(a,b)). The effect of pH values on the fluorescence intensity of **L₁** and **1** is also examined and shown in Supplementary Fig. S19(c,d)).

DNase and RNase digestion test. After exploring the specific nucleus and nucleolus staining capability of **1**, it is anticipated that **1** must specifically bind to nucleic acid. The mechanistic pathways and reason of specific nucleus and nucleolus staining by **1** is hypothesized by binding of **1** with DNA and RNA in the nucleus and nucleolus, respectively. The intracellular nucleic acid binding is explored by a deoxyribonuclease (DNase) and ribonuclease (RNase) digestion test[44] and the results can be visualized in Fig. 7. HeLa and MCF-7 cell lines were stained with **1** and subsequently treated with DNase and RNase. Since, DNase hydrolyze only DNA substrate in the cells,

the fluorescence of the nucleus is vanished while the nucleolus is found glowing in DNase treated cells, which confirmed the interaction of **1** with DNA present in the cell nucleus as evident in Fig. 7. Similarly, the RNase hydrolyze only the RNA substrate in the cells, resulting in no fluorescence from the nucleolus and the weak cytoplasmic fluorescence has also vanished while the nucleus was glowing in RNase treated cells, which approved the interaction of **1** with RNA present in the cells. The DNA binding of **1** is also validated by EtBr displacement assay and the results are shown in Supplementary Fig. S20. These observations supported the hypothesis of nucleic acid binding of **1** resulting into specific cellular localization and nucleus and nucleoli staining.

The photostability of **1** was studied in live cells and was compared with Hoechst and FITC. The intensity of FITC and Hoechst was reduced to 30% of the initial intensity after 1500 scans while the fluorescence from **1** was almost consistent and was clearly visible upto 3600 scans studied. (Supplementary Fig. S21).

The existence of RNA selective compounds is limited. One of the reasons is better affinity of small molecules towards double stranded DNA than single stranded RNA[45]. Also, the complicated environment of living cells, sometimes results in non-specific binding and imaging. SYTO RNA-Select is the only commercially available live cell RNA staining dye. Another existing limitation comes from photo-bleaching and self–quenching of nucleus and nucleolus staining agents. The present work successfully overcomes these limitations and reports a nucleic acid specific compound which stains both the nucleus and the nucleolus with better photostability.

Discussion

In summary, we for the first time report the specific staining of nucleus and nucleoli by **1**, which is prepared in a facile manner. The ligand **L₁** involved in synthesis of **1** also promotes selective and sensitive sensing of Al^{3+}. **1** is explored for specific nucleic acid binding using DNA and RNA digestion and employed as a specific nucleus and nucleolus staining agent. Our results are expected to inspire replacement of existing expensive and sensitive nucleic acid specific dyes. Use of **1** for both nucleus and nucleoli staining can be of great scientific interest.

Methods

Synthesis of chemosensor (L₁). 2,4,6-trimethylbenzene-1,3-diamine (0.189 g, 1 mmol) dissolved in dry methanol (10 ml) was added to a solution of 2-Hydroxy-1-napthaldehyde (0.172 g, 1 mmol) in methanol (15 ml). The content of the flask heated under reflux for 3 h. A yellow oily compound was formed which is monitored by TLC. Solvent was evaporated on *vacuo* and washed with hexane. A yellow solid was obtained which was dried under vacuum. Needle shaped yellow crystals were suitable for single crystal X-ray analyses were obtained by recrystallization from methanol-chloroform (2:1) within two days. Characterization data. ^1H NMR (400 MHz, CDCl₃): δ15.27(s, 1H), 8.96(s, 1H, −CH=N), 7.92(d, J = 8Hz, 1H), 7.80(d, J = 8Hz, 1H), 7.71(d, J = 8Hz, 1H), 7.45(t, J = 8Hz, 1H), 7.30(t, J = 8Hz, 1H), 7.45(s, 1H), 7.11(d, J = 8Hz.1H), 6.89(s, 1H), 3.(s, 2H), 2.20(s, 3H), 2.19(s, 3H), 2.13(s, 3H).). ^{13}C NMR (400 MHz, CDCl3): δ170.10, 160.67, 143.05, 141.51, 136.25, 133.36, 129.86, 129.25, 128.00, 127.04, 123.22, 122.36, 119.74, 119.08, 118.51, 114.19, 108.4, 17.98, 17.45, 12.60. IR (KBr, cm⁻¹): 3447(br), 2360(w), 1620(vs), 1532(w), 1475(w), 1311(w), 1093(w), 838(w), 746(w). λ_{max} = 310, 360 nm, HRMS (m/z): [M] calcd. for $C_{20}H_{20}N_2O$, 305.16; found, 305.13; analysis (calcd., found for $C_{20}H_{20}N_2O$): C(77.57, 78.92), H(6.73, 6.62), N(9.85, 9.20).

Synthesis of 1. A methanolic solution (10 mL) of $Al(NO_3)_2.9H_2O$ (0.375g 1 mmol) was added dropwise with stirring to a solution of **L₁** (0.304g 1 mmol) in methanol (10 mL). The reaction mixture was stirred for additional 6 h, washed with Diethyl ether twice and evaporated on *vacuo*. Characterization data: ^{27}Al NMR (400 MHz, DMSO-D6): δ 3.34; HRMS (m/z): [M] calcd. for $C_{21}H_{25}AlN_4O_9$, 503.43; found, 502.98; λ_{max} = 419, 360 and 309 nm.

Nucleus specific staining. Breast cancer cell line MCF-7, cervical cancer cell line HeLa and skin melanoma A375 were seeded in confocal dishes. Adherent cells were stained with Hoescht 33342 (50 μg/mL) and incubated for 15 minutes at at 37 °C in 5% CO_2. The cells were rinsed with PBS thrice and was visualised under confocal microscope at an excitation of $\lambda_{ex.}$ = 405nm and $\lambda_{ex.}$ = 488nm. Without changing the positioning of cells under microscope, cells were stained with **1** (30 μM) and kept for 10 minutes. Further the cells were visualised using confocal microscope at $\lambda_{ex.}$ = 488nm.

DNase and RNase digestion tests. MCF-7 and HeLa cell lines were first seeded in confocal dishes. The cells were fixed by cold methanol (HPLC grade) for 1 min. Further, the cells were treated with 1% Triton X-100 to make the cell membrane permeabilized. The cells were rinsed thrice with 1X PBS to remove the leftover detergent. Afterwards, cells were stained with 30 μM **1**. After staining cells were rinsed with PBS thrice. Blank PBS (as control experiment), 50 mg/ml DNase or 75 mg/ml RNase was added into different confocal dishes containing cells and kept in an incubator at 37 °C in 5% CO_2 for 3 hr. Further, the cells were subjected to confocal microscopy.

Physical measurements. ^1H NMR (400 MHz), and ^{13}C NMR(100 MHz) spectra were recorded on the Bruker Avance (III) instrument by using CDCl₃.^1H NMR chemical shifts are reported in parts per million (ppm) relative to the solvent residual peak (CDCl₃, 7.26 ppm). ^{13}C NMR chemical shifts are reported relative to the solvent residual peak (CDCl₃, 77.36 ppm). IR spectra [4000−400 cm⁻¹] were recorded with a Bio-Rad FTS 3000MX instrument on KBr pellets. Elemental analyses were carried out with a Thermo-Flash 2000 elemental analyser. Spectrophotometric measurement were performed on a varian UV-vis spectrophotometer (model: Cary 100) using a quartz cuvette with a path length of 1cm. The excitation and emission slits were 5/5 nm for the emission measurements. The mass spectra were recorded on Brucker-Daltonics, micrOTOF-QII mass spectrometer. The life time measurement recorded on TCSPC system from Horiba Yovin (Model: Fluorocube-01-NL). The samples were excited at 375 nm using a picosecond diode laser (Model: Pico Brite-375L) with the repetition rate of 5 MHz. The signals were collected at magic angle (54.70) polarization using a photomultiplier tube (TBX-07C) as

detector, which has a dark counts less than 20 cps. The instrument response function of our setup was 150 ps. The data analysis was performed using IBH DAS (version 6, HORIBA Scientific, Edison, NJ) decay analysis software. NMR spectra of **L₁** and **1** are depicted in Supplementary Figs S22–S25.

References

1. Rivera-Fuentes, P. & Lippard, S. J. Metal-Based Optical Probes for Live Cell Imaging of Nitroxyl (HNO). *Acc. Chem. Res.* **48,** 2927–2934 (2015).
2. Carter, K. P., Young, A. M. & Palmer, A. E. Fluorescent Sensors for Measuring Metal Ions in Living Systems. *Chem. Rev.* **114,** 4564–4601 (2014).
3. Chyan, W., Zhang, D. Y., Lippard, S. J. & Radford, R. J. Reaction-based fluorescent sensor for investigating mobile Zn^{2+} in mitochondria of healthy versus cancerous prostate cells. *Proc. Natl. Acad. Sci.* **111,** 143–148 (2014).
4. Xu, R. *et al.* Nanoscale Metal–Organic Frameworks for Ratiometric Oxygen Sensing in Live Cells. *J. Am. Chem. Soc.* **138,** 2158–2161 (2016).
5. Sharma, V., Saini, A. K. & Mobin, S. M. Multicolour fluorescent carbon nanoparticle probes for live cell imaging and dual palladium and mercury sensors. *J. Mater. Chem. B* **4,** 2466–2476 (2016).
6. Kim, S. *et al.* Salicylimine-Based Fluorescent Chemosensor for Aluminum Ions and Application to Bioimaging. *Inorg. Chem.* **51,** 3597–3602 (2012).
7. Fasman, G. D. Aluminum and Alzheimer's disease: model studies. *Coord. Chem. Rev.* **149,** 125–165 (1996).
8. Nayak, P. Aluminum: Impacts and Disease. *Environ. Res.* **89,** 101–115 (2002).
9. Cronan, C. S., Walker, W. J. & Bloom, P. R. Predicting aqueous aluminium concentrations in natural waters. *Nature* **324,** 140–143 (1986).
10. Berthon, G. Aluminium speciation in relation to aluminium bioavailability, metabolism and toxicity. *Coord. Chem. Rev.* **228,** 319–341 (2002).
11. Valeur, B. & Leray, I. Design principles of fluorescent molecular sensors for cation recognition. *Coord. Chem. Rev.* **205,** 3–40 (2000).
12. Gupta, V. K., Shoora, S. K., Kumawat, L. K. & Jain, A. K. A highly selective colorimetric and turn-on fluorescent chemosensor based on 1-(2-pyridylazo)-2-naphthol for the detection of aluminium(III) ions. *Sens. Actuators B Chem.* **209,** 15–24 (2015).
13. Sen, S. *et al.* A water soluble Al3+ selective colorimetric and fluorescent turn-on chemosensor and its application in living cell imaging. *Analyst* **137,** 3975–3981 (2012).
14. Liu, S. *et al.* A multifunctional phosphorescent iridium(III) complex for specific nucleus staining and hypoxia monitoring. *Chem. Commun.* **51,** 7943–7946 (2015).
15. Gill, M. R. *et al.* A ruthenium(II) polypyridyl complex for direct imaging of DNA structure in living cells. *Nat. Chem.* **1,** 662–667 (2009).
16. Kang, Y.-F., Fang, Y.-W., Li, Y.-H., Li, W. & Yin, X.-B. Nucleus-staining with biomolecule-mimicking nitrogen-doped carbon dots prepared by a fast neutralization heat strategy. *Chem. Commun.* **51,** 16956–16959 (2015).
17. Wang, X. *et al.* Steering graphene quantum dots in living cells: lighting up the nucleolus. *J. Mater. Chem. B* **4,** 779–784 (2016).
18. Maity, D. & Govindaraju, T. Pyrrolidine constrained bipyridyl-dansyl click fluoroionophore as selective Al3+ sensor. *Chem. Commun.* **46,** 4499–4501 (2010).
19. Wang, Y.-W. *et al.* A colorimetric and fluorescent turn-on chemosensor for Al3+ and its application in bioimaging. *Tetrahedron Lett.* **50,** 6169–6172 (2009).
20. Samanta, S., Goswami, S., Hoque, M. N., Ramesh, A. & Das, G. An aggregation-induced emission (AIE) active probe renders Al(III) sensing and tracking of subsequent interaction with DNA. *Chem. Commun.* **50,** 11833–11836 (2014).
21. Boyer, P. D. *et al.* Delivering Single-Walled Carbon Nanotubes to the Nucleus Using Engineered Nuclear Protein Domains. *ACS Appl. Mater. Interfaces* **8,** 3524–3534 (2016).
22. Kong, W. *et al.* High-bright fluorescent carbon dots and their application in selective nucleoli staining. *J. Mater. Chem. B* **2,** 5077–5082 (2014).
23. Ai, J. *et al.* Multifunctional near-infrared fluorescent nanoclusters for simultaneous targeted cancer imaging and photodynamic therapy. *Sens. Actuators B Chem.* **222,** 918–922 (2016).
24. Liu, W. *et al.* Deep-Red Emissive Crescent-Shaped Fluorescent Dyes: Substituent Effect on Live Cell Imaging. *ACS Appl. Mater. Interfaces* **7,** 7421–7427 (2015).
25. Zhou, B. *et al.* Imaging of nucleolar RNA in living cells using a highly photostable deep-red fluorescent probe. *Biosens. Bioelectron.* **68,** 189–196 (2015).
26. Yu, J., Parker, D., Pal, R., Poole, R. A. & Cann, M. J. A Europium Complex That Selectively Stains Nucleoli of Cells. *J. Am. Chem. Soc.* **128,** 2294–2299 (2006).
27. Zhang, K. Y. *et al.* Structure, Photophysical and Electrochemical Properties, Biomolecular Interactions, and Intracellular Uptake of Luminescent Cyclometalated Iridium(III) Dipyridoquinoxaline Complexes. *Inorg. Chem.* **49,** 2530–2540 (2010).
28. Shen, R. *et al.* Multifunctional Conjugates To Prepare Nucleolar-Targeting CdS Quantum Dots. *J. Am. Chem. Soc.* **132,** 8627–8634 (2010).
29. Li, D. *et al.* Nucleic acid-selective light-up fluorescent biosensors for ratiometric two-photon imaging of the viscosity of live cells and tissues. *Chem. Sci.* **7,** 2257–2263 (2016).
30. Saini, A. K., Srivastava, M., Sharma, V., Mishra, V. & Mobin, S. M. A highly selective, sensitive and reversible fluorescence chemosensor for Zn^{2+} and its cell viability. *Dalton Trans.* **45,** 3927–3935 (2016).
31. Mobin, S. M., Mishra, V. & Chaudhary, A. Isolation of a Metastable Intermediate in a Heterometallic CuII–HgII 1D Polymeric Chain: Synthesis, Crystal Structure, and Photophysical Properties. *Inorg. Chem.* **54,** 1293–1299 (2015).
32. Kwon, J. E. *et al.* Fluorescent Zinc Sensor with Minimized Proton-Induced Interferences: Photophysical Mechanism for Fluorescence Turn-On Response and Detection of Endogenous Free Zinc Ions. *Inorg. Chem.* **51,** 8760–8774 (2012).
33. Ashokkumar, P., Ramakrishnan, V. T. & Ramamurthy, P. Photoinduced Electron Transfer (PET) Based Zn2+ Fluorescent Probe: Transformation of Turn-On Sensors into Ratiometric Ones with Dual Emission in Acetonitrile. *J. Phys. Chem. A* **115,** 14292–14299 (2011).
34. Zhang, J. F., Zhou, Y., Yoon, J. & Kim, J. S. Recent progress in fluorescent and colorimetric chemosensors for detection of precious metal ions (silver, gold and platinum ions). *Chem. Soc. Rev.* **40,** 3416–3429 (2011).
35. Benesi, H. A. & Hildebrand, J. H. A Spectrophotometric Investigation of the Interaction of Iodine with Aromatic Hydrocarbons. *J. Am. Chem. Soc.* **71,** 2703–2707 (1949).
36. Shiraishi, Y., Sumiya, S., Kohno, Y. & Hirai, T. A Rhodamine–Cyclen Conjugate as a Highly Sensitive and Selective Fluorescent Chemosensor for Hg(II). *J. Org. Chem.* **73,** 8571–8574 (2008).
37. Rajamalli, P. & Prasad, E. Low Molecular Weight Fluorescent Organogel for Fluoride Ion Detection. *Org. Lett.* **13,** 3714–3717 (2011).
38. Lin, Q. *et al.* Rationally designed anion-responsive-organogels: sensing F− via reversible color changes in gel–gel states with specific selectivity. *Soft Matter* **10,** 5715–5723 (2014).
39. Lin, Q. *et al.* A highly selective and sensitive fluorescence 'turn-on' fluoride ion sensor. *RSC Adv.* **5,** 11786–11790 (2015).
40. Carmichael, J., DeGraff, W. G., Gazdar, A. F., Minna, J. D. & Mitchell, J. B. Evaluation of a tetrazolium-based semiautomated colorimetric assay: assessment of chemosensitivity testing. *Cancer Res.* **47,** 936–942 (1987).

41. Wallrabe, H. & Periasamy, A. Imaging protein molecules using FRET and FLIM microscopy. *Curr. Opin. Biotechnol.* **16,** 19–27 (2005).
42. Suhling, K., French, P. M. W. & Phillips, D. Time-resolved fluorescence microscopy. *Photochem. Photobiol. Sci.* **4,** 13–22 (2005).
43. wang, L. & Zhou, H. S. Green synthesis of luminescent nitrogen-doped carbon dots from milk and its imaging application. *Anal. Chem.* **86,** 8902–8905 (2014).
44. Lu, Y.-J. *et al.* A molecular fluorescent dye for specific staining and imaging of RNA in live cells: a novel ligand integration from classical thiazole orange and styryl compounds. *Chem. Commun.* **51,** 15241–15244 (2015).
45. Chang Y. T., Li Q. & Rosania G. inventors; New York University, assignee. RNA-selective styryl probes for live cell imaging of nuclear structure and function. United States patent US 7,790,896. Sept 7, 2010.

Acknowledgements

Author Contributions

P.M. and M.M.S. supervised the project. A.K.S. and V.S. performed the experiments and compiled the data. The manuscript was written through contributions of all authors. All authors have given approval to the final version of the manuscript.

Additional Information

Supplementary information accompanies this paper at http://www.nature.com/srep

Competing financial interests: The authors declare no competing financial interests.

How to cite this article: Saini, A. K. *et al.* The development of fluorescence turn-on probe for Al(III) sensing and live cell nucleus-nucleoli staining. *Sci. Rep.* **6**, 34807; doi: 10.1038/srep34807 (2016).